A 4DVAR System for the Navy Coastal Ocean Model. Part II: Strong and Weak Constraint Assimilation Experiments with Real Observations in Monterey Bay*

HANS NGODOCK AND MATTHEW CARRIER

Naval Research Laboratory, Stennis Space Center, Mississippi

(Manuscript received 9 July 2013, in final form 20 December 2013)

ABSTRACT

A four-dimensional variational data assimilation (4DVAR) system was recently developed for the Navy Coastal Ocean Model (NCOM). The system was tested in the first part of this study using synthetic surface and subsurface data. Here, a full range of real surface and subsurface data is considered following encouraging results from the preliminary test. The data include sea surface temperature and sea surface height from satellite, as well as subsurface observations from gliders deployed during the second Autonomous Ocean Sampling Network field experiment in California's Monterey Bay. Data assimilation is carried out with strong and weak constraints, and results are compared against independent observations. This study clearly shows that the 4DVAR approach improves the free-running model simulation and that the weak constraint experiment has lower analysis errors than does the strong constraint version.

1. Introduction

Following up on promising results in Ngodock and Carrier (2014, hereafter Part I) from the assimilation of synthetic observations in the Monterey Bay of California using a four-dimensional variational data assimilation (4DVAR) system developed for the Navy Coastal Ocean Model (NCOM), consideration is now given to real observations. The assimilation of synthetic observations was intended to test the functionality of the 4DVAR system and its ability to fit the observations and correct erroneous external forcing fields. The system is used here to assimilate observations from the second Autonomous Ocean Sampling Network (AOSN II), an oceanographic data campaign that took place in Monterey Bay from 23 July to 6 September 2003 and that was supported by a nowcast effort from three modeling groups: the Harvard Ocean Prediction System (HOPS; Robinson et al. 1996; Robinson 1999; Haley et al. 1999), the Regional Oceanic Modeling System (ROMS; Shchepetkin and McWilliams 2005), and NCOM (Martin 2000; Barron et al. 2004, 2006).

Monterey Bay is an interesting region for ocean modeling due to a complex coastline with steep topography, strong land–sea-breeze patterns, and the existence of frequent local upwelling and relaxation events (Shulman et al. 2002). The region is also home to regular observation campaigns. According to Ramp et al. (2009), other factors making Monterey Bay an ideal location for such an experiment as AOSN II are its close proximity to several large research institutions; ship availability; the wealth of environmental and scientific problems presented; the wide continental shelves within and to the north of the bay providing a strong contrast to the nearby deep water within the Monterey Bay Submarine Canyon (MSC) and the narrower, steeper shelf to the south; and finally the two upwelling centers at Point Sur and Cape Año Nuevo, which are both within a day's steam by research vessel.

The real-time analysis and forecast support of the AOSN II field experiment was followed by reanalysis data experiments by several authors (Haley et al. 2009; Chao et al. 2009; Shulman et al. 2009). The general conclusion from these experiments is that the reanalysis was in better agreement with both the assimilated and independent temperature and salinity observations after some model parameters were adjusted. The same fit was worse in the real-time support of the field experiment.

* Naval Research Laboratory Contribution Number JA/7320-13-13-1822.

Corresponding author address: Hans Ngodock, Naval Research Laboratory, Code 7321, Stennis Space Center, MS 39529.
E-mail: hans.ngodock@nrlssc.navy.mil

DOI: 10.1175/MWR-D-13-00220.1

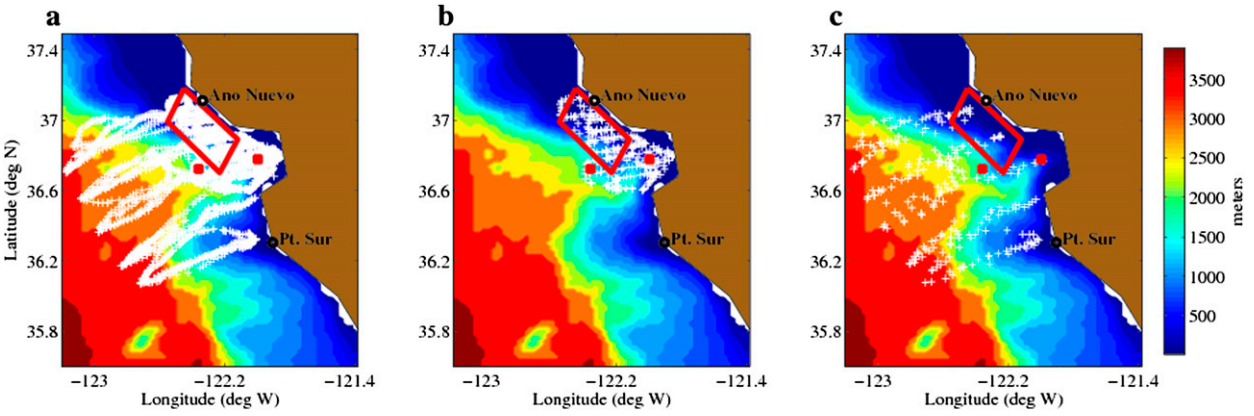

FIG. 1. (a) All gliders and the two mooring positions, and assimilated (b) Slocum and (c) Spray glider tracks during August 2003. The red dots represent the locations of the moored buoys M1 (inside the bay) and M2 (offshore), and the red box represents the Año Nuevo upwelling center.

Also, the surface velocity field derived from the reanalysis could only qualitatively resemble the one observed by HF radar stations, with the amplitude and position of current features sometimes found to be erroneous (Haley et al. 2009; Chao et al. 2009).

It is worth noting that in both real time and reanalyses with the AOSN II dataset all the experiments used a sequential data assimilation technique: the error subspace statistical estimation of Lermusiaux et al. (2002), the three-dimensional variational data assimilation (3DVAR) scheme (Chao et al. 2009), or the multivariate optimal interpolation of Cummings (2005) used in Shulman et al. (2009, 2010). None was carried out with a 4DVAR-type scheme. In this study, the same dataset will be assimilated using the 4DVAR algorithm based on the representer method that was developed for the Navy Coastal Ocean Model. Of particular interest is the ability of the 4DVAR system to overcome the shortcomings of the sequential methods through its ability to fit the observations without adjusting the model parameters. The 4DVAR system will seek to adjust either the initial conditions (strong constraints) or the model forcing (weak constraints), or both, by exploiting flow-dependent correlations defined by the integration of the adjoint and tangent linear models.

Coastal upwelling and relaxation, as well as the mesoscale variability were the main physical processes of interest for the observation campaign. Upwelling and relaxation events play a major role in the ocean dynamics in and around Monterey Bay. Upwelling is the ocean's response to northwesterly winds, and relaxation occurs as the winds weaken and/or change direction. These upwelling and relaxation events occur mainly around two so-called upwelling centers: Año Nuevo to the northwest of the bay and around Point Sur to the south of the bay. Surface wind observations at the Monterey Bay Aquarium Research Institute moorings M1 and M2 during August 2003 show that upwelling-favorable winds prevailed from 7 to 19 August, followed by relaxation-favorable winds from 20 to 25 August, when upwelling-favorable winds returned (Shulman et al. 2010). The locations of the M1 and M2 buoys are shown in Fig. 1, along with glider tracks. Several Slocum and Spray gliders sampled the Año Nuevo upwelling center during the transitions from upwelling to relaxation and back to upwelling, providing observations that allow the assessment of the model and assimilation performance during those events.

A time series of observed and modeled wind barbs at M1 and M2 is shown in Fig. 2, along with the observed and modeled SST. It can be seen in Fig. 2 that upwelling is associated with the decrease in surface temperature following northwesterly winds. Relaxation follows when the wind pattern is altered or reversed and is associated with the rise of surface temperature. The correlation between the wind and surface temperature patterns seems to be stronger at M1 than at M2. The wind direction suggests that the upwelled waters around Año Nuevo are flowing toward M1. Therefore, the assimilation solutions will be evaluated at M1 to ensure that the prevalent dynamics of the region are preserved by the assimilation system; that is, the fit to the observations is not accomplished at the expense of the dynamics. Both wind direction and temperature patterns observed at M1 show that there is an upwelling event from 5 to 15 August, as well as a relaxation event from 15 to 23 August. From 23 to 25 August there is a short-lived upwelling followed by a short-lived relaxation, and from 25 August to the end of the assimilation window there is only an upwelling event.

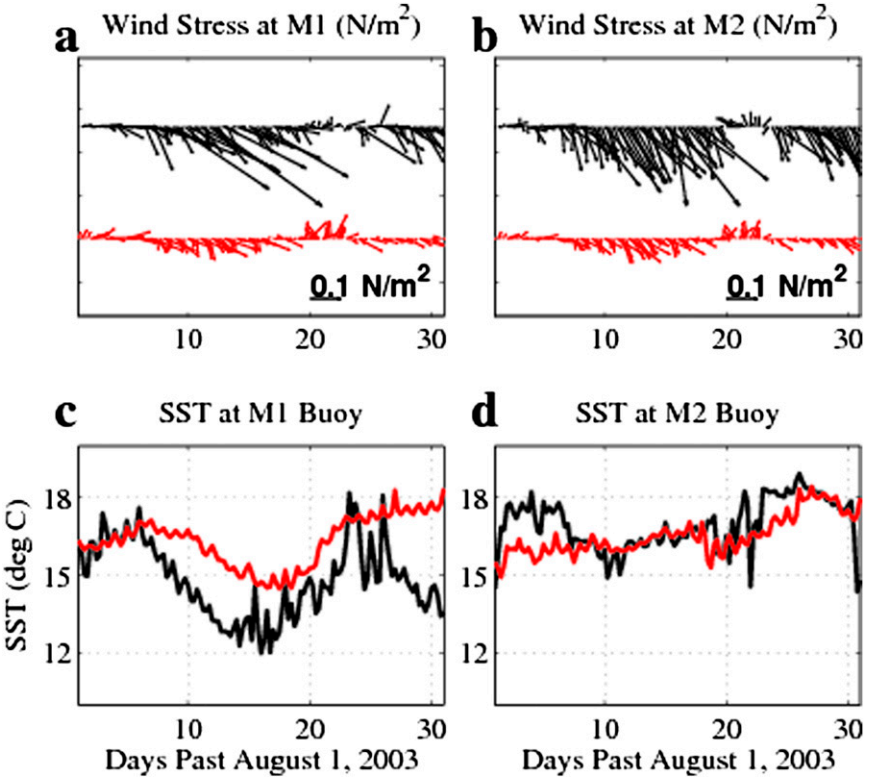

FIG. 2. Observed (black) and modeled (red) (a),(b) wind barbs at the M1 and M2 buoy locations and (c),(d) surface temperature.

It was suggested in Part I of this study that the assimilation system was able to fit the observations with low prescribed model errors while the free run had relatively high errors prescribed to the model forcing fields. The study here aims to demonstrate the robustness of the assimilation system in its ability to accurately fit assimilated and nonassimilated real observations and dynamics of Monterey Bay with low model errors as well.

Brief descriptions of the dataset and the assimilation system are given in sections 2 and 3, respectively, followed by the assimilation experiment results in section 4. Concluding remarks are given in section 5.

2. Data

The dataset used in this study consists of SST from satellite and aircraft, a few sea surface heights (SSHs) from satellite altimetry (due to the limited area of the model domain), vertical profiles of temperature and salinity from Slocum and Spray gliders and two moorings (M1 and M2), and AXBTs. All the vertical profiles are projected onto a static grid of 50 levels. The observations are obtained through the operational Navy Coupled Ocean Data Assimilation (NCODA) system by Cummings (2005), which also contains a data acquisition and quality control component. The SSH observations are not assimilated because only a few distant observations appear sporadically in the domain every 2–3 days. On the other hand, the majority of the SST observations are from the Geostationary Operational Environmental Satellite (GOES) series, with a spatial resolution of about 6 km in the absence of cloud cover.

Slocum glider tracks covered a portion of the bay, the mouth of the bay, and the area to the northwest of the bay (i.e., the upwelling center around Año Nuevo). Spray glider tracks originated from the nearshore and went offshore in transectlike trajectories, as seen in Fig. 1. As a result of the sampling frequency of the gliders, many observations are adjacent to each other along glider tracks. To avoid redundancy, some of the glider data are withheld from the assimilation and are used for validation of the analyses, as is also the case for the mooring M1. Withholding the data takes into account the model grid resolution and the prescribed horizontal and temporal decorrelation scale of the model error in such a way that only one data point is retained within one-and-a-half decorrelation scale at any given time. The observations are assigned a constant error of 0.4 K and 0.1 psu in temperature and salinity, respectively.

3. Experiments and results

The 4DVAR assimilation system was described in Part I. It has the flexibility to carry out experiments with either strong constraints using a gradient descent approach or weak constraints using the indirect representer method (Bennett 1992, 2002). Smaller error variances and shorter spatial (30 km) and longer temporal (3 days) decorrelation scales are adopted for the assimilation of the AOSN II data.

The assimilation covers the time window from 1 to 31 August 2003, and is carried out in cycles of 5 days, with the analysis at the end of a cycle becoming the initial conditions for the following cycle. Observations are processed and stored in 6-h intervals, and the 4DVAR system assimilates all observations within each 5-day cycle. The performance of the assimilation system is examined by computing the difference between the observations and three model solutions: (i) the free-running (nonassimilative) model that is integrated from the given initial conditions and forcing fields; (ii) the first guess (also nonassimilative), for which the initial conditions are updated from the assimilation in the previous cycle, with the exception of the first cycle where both the first guess and the free-running model are equal; and (iii) the analysis. The first guess (not shown) is also the background trajectory for the tangent linear model and the adjoint (i.e., the trajectory around which the model is linearized). It is stored in intervals of 6 h. It is expected of every assimilation system to fit the assimilated observations within one observation standard deviation. Unassimilated observations consist of withheld observations within the current assimilation window and future observations, that is, those in the next cycle before the assimilation. The assimilation is expected to fit the former as a measure of the system's ability to propagate the information from the assimilated observations sites through the model's space–time domain within the assimilation window. However, there is no expectation to fit future observations; that is, the innovations in the next cycle are not expected to be smaller than the observation standard deviation. One only hopes that having initialized the model from the previous cycle's assimilation, the model forecast will remain sufficiently accurate to maintain small innovations, given an accurate external forcing.

There are two assimilation experiments presented in this work. First, a strong constraint 4DVAR experiment is set up on the assumption that the discrepancy between the model and the observations is solely due to erroneous initial conditions. This is done in part because it was reported by Haley et al. (2009) that the atmospheric forcing fields provided by the Coupled Ocean–Atmosphere Mesoscale Prediction System (COAMPS) were mostly in agreement with local independent observations. The strong constraint is achieved by setting the model error to zero in the representer algorithm. Thus, the initial increments are propagated forward in time using linearized dynamics. Because the assimilation window is within the time range of validity of the tangent linear approximation, this approach is expected to yield similar results to the traditional strong constraints where the initial condition increments are propagated through the nonlinear model. The second experiment is the weak constraint assimilation using the representer algorithm, with model errors prescribed in addition to the initial condition errors. Although the COAMPS wind forcing field is in good agreement with local buoys, it can have errors of about $2\,\mathrm{m\,s^{-1}}$, that is, 100% of the wind stress, according to Kindle et al. (2002) and Haley et al. (2009). In addition, Shulman et al. (2009) suggested that the daily average atmospheric solar heat flux can be in error by as much as $29–36\,\mathrm{W\,m^{-2}}$ and that on any given day the error may be much higher, between 50 and $90\,\mathrm{W\,m^{-2}}$, which is roughly 12%–20% of the total heat flux. Initial condition errors for temperature, salinity, velocity, and SSH are 2 K, 0.5 psu, $0.52\,\mathrm{m\,s^{-1}}$, and 0.1 m, respectively. The model errors in the assimilation system are 20% of the heat flux, 5% of the salinity flux, and 5% of the wind stress.

a. *Fitting the assimilated observations*

Assimilation results are shown for the upper 200 m, which seems to be the active layer according to Liang and Robinson (2009). The differences between the observations and the model are computed for all assimilated profiles of temperature and salinity and plotted in chronological order in Fig. 3. It can be seen that the temperature differences are confined in the upper 100 m of the water column, with magnitudes sometimes reaching 3 K for the free run. Salinity differences extend deeper in the water column, to about 200 m, although the largest differences are also confined to the upper 100 m. The assimilation is able to significantly reduce the free-run discrepancies in both the temperature and salinity fields, with the exception of a few profiles. The assimilation is able to reduce discrepancies as high as 3 K and 0.4 psu to less than 0.5 K and 0.1 psu in temperature and salinity, respectively. There are only a few noticeable differences between the strong and weak constraint analysis residuals; they both fit the assimilated glider data with similar accuracy.

b. *Upwelling center*

The Año Nuevo upwelling center was sampled almost exclusively by the Slocum gliders. The ability of the

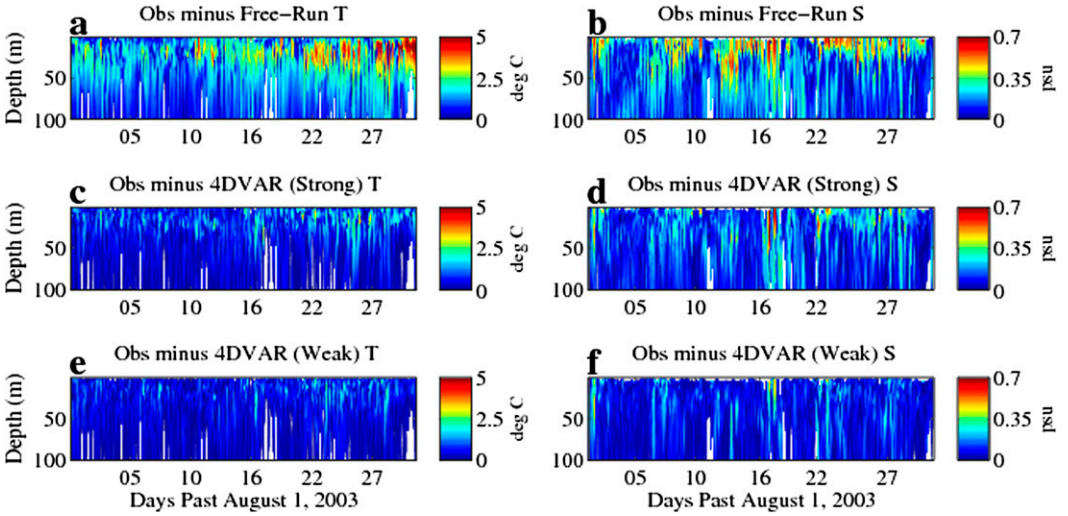

FIG. 3. Absolute model (left) temperature and (right) salinity discrepancies compared to assimilated observations for (a),(b) the free run, and the (c),(d) strong and (e),(f) weak constraint analyses. The residuals are computed for all assimilated glider data.

assimilation system to correct the model deficiencies in simulating the upwelling and relaxation events is assessed by examining the analysis residuals for the Slocum gliders only.

It can be seen in Fig. 4 that temperature discrepancies from the free run were moderate during the first upwelling and relaxation events (i.e., 20 August). Temperature discrepancies increased from the end of the relaxation event through the short-lived upwelling and relaxation events between 22 and 25 August, as mentioned earlier, and the discrepancies kept growing until the end of the assimilation window. The salinity discrepancies are rather low throughout the assimilation window, with only a few noticeable profiles where the free run departs from the observations by 0.4 psu. The strong constraint assimilation fits most of the Slocum temperature and salinity profiles remarkably well. Only a few isolated profiles (e.g., temperature during the short-lived upwelling and relaxation events around 25 August, and salinity profiles around 13 and 22 August) have analysis residuals greater than the observation standard deviation. Most of these residuals are further reduced in the weak constraint assimilation, with the exception of the salinity profile around 13 August. Thus, the assimilation system is able to correct the model trajectory so that it fits the observations of the upwelling and relaxation events in both the strong and weak constraint experiments.

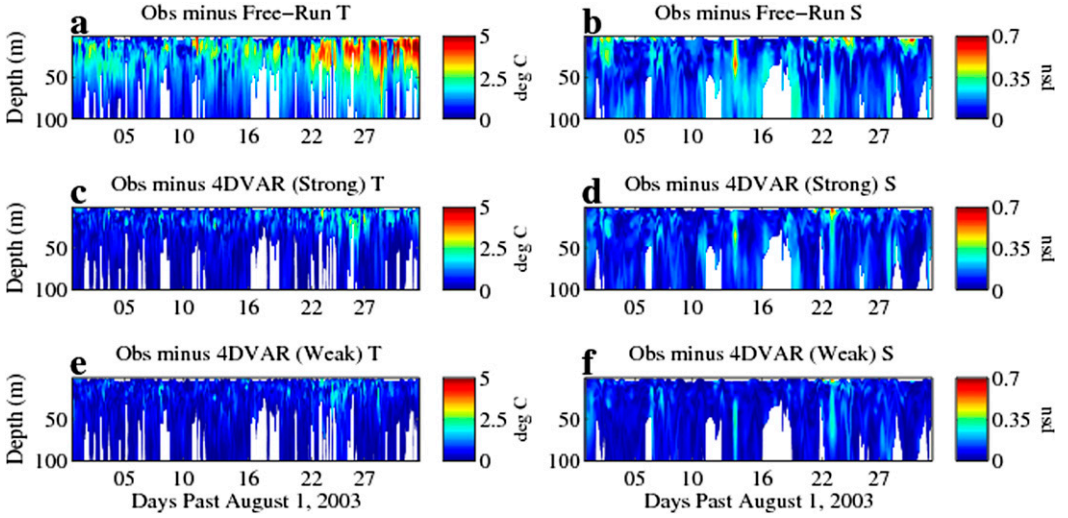

FIG. 4. As in Fig. 3, but for Slocum gliders only.

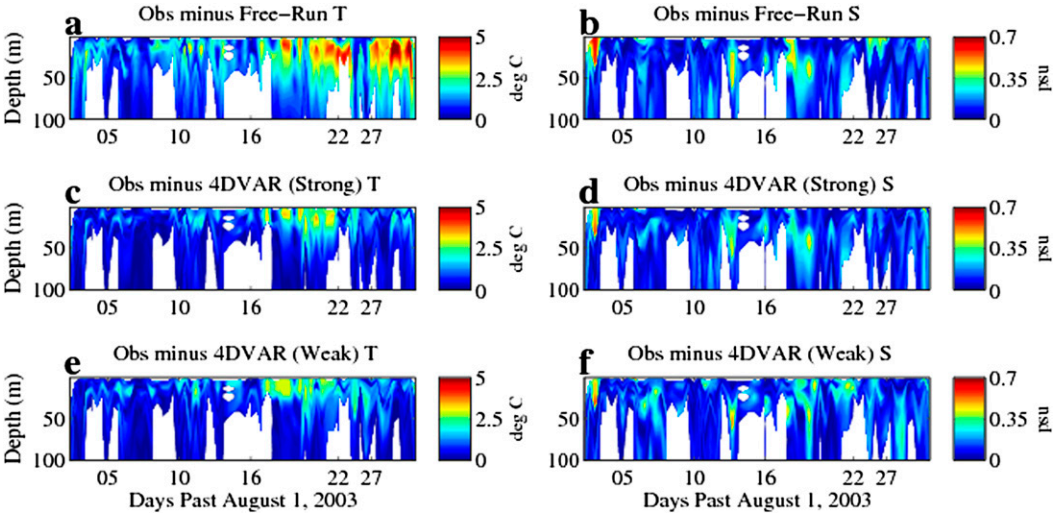

FIG. 5. As in Fig. 3, but for nonassimilated Slocum glider observations.

c. *Independent observations*

For verification and evaluation purposes, discrepancies are computed between the withheld glider observations and the three model solutions: the free run, and the strong and the weak constraint analyses. Results are shown in Fig. 5 for the withheld Slocum glider data for the main reason that these are the gliders that mostly sampled the upwelling center of Año Nuevo. It can be seen that both strong and weak constraint analyses generally fit these nonassimilated observations with the same level of accuracy. This result was expected because in most cases the withheld observations were located in the vicinity of assimilated observations.

In addition to the withheld glider observations, the model solutions were also compared to the unassimilated observations collected at the M1 and M2 moored buoys, with results shown in Fig. 6 for M1.

At the M1 buoy the free-run solution has moderate to high temperature discrepancies from the beginning of the assimilation window to the onset of the three rapid transitions from relaxation to upwelling to relaxation and to another upwelling event between 22 and 25 August. These discrepancies grow subsequently as evidence of the model diverging from the independent observations, as was the case along the Slocum glider tracks. The temperature discrepancies of the analyses show that both the strong and weak constraint assimilations are able to accurately reproduce the observed temperatures at M1.

In stark contrast with temperature, salinity discrepancies from the free run show that the model salinity begins to diverge from the independent observations 2 days

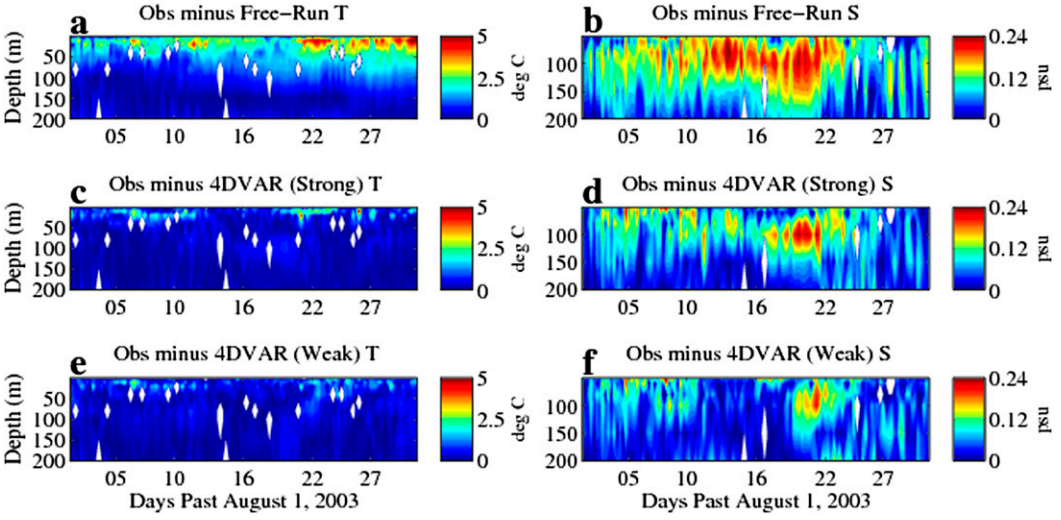

FIG. 6. As in Fig. 5, but for buoy M1.

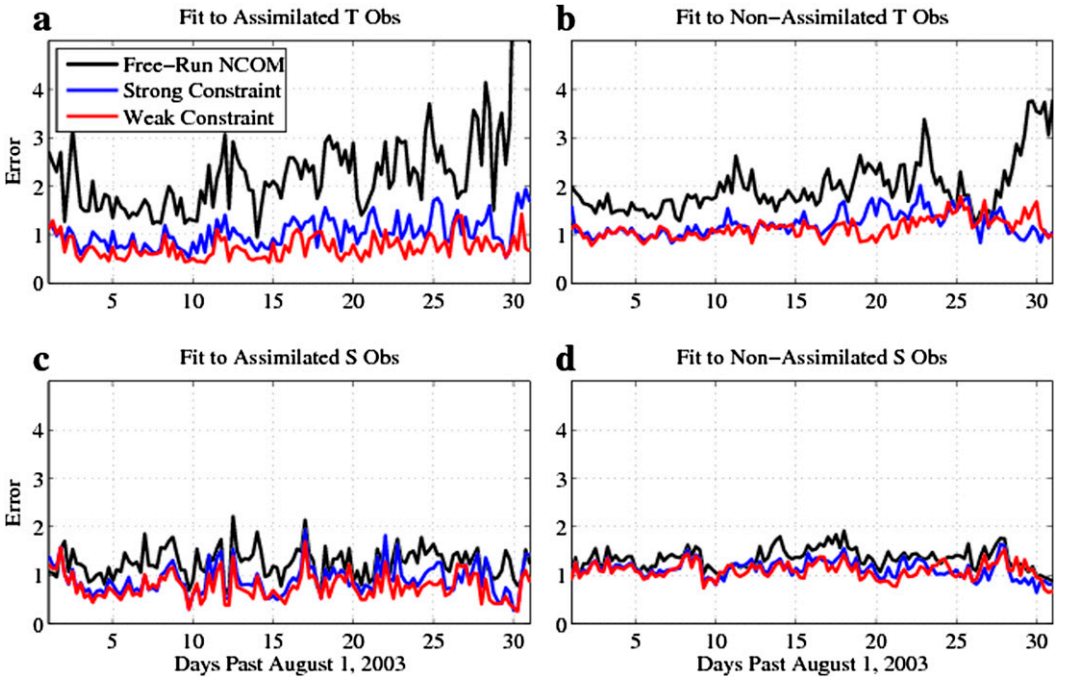

FIG. 7. Fit to (a),(b) the assimilated and nonassimilated temperature and (c),(d) the assimilated and nonassimilated salinity observations for the free run (black), and the strong (blue) and weak (red) constraint analyses.

into the assimilation window with growing errors until 23 August, right before the rapid transitions mentioned above. In addition, the salinity discrepancies extend deeper into the water column. The analysis discrepancies show that the strong constraint assimilation was able to significantly but not completely reduce the errors, particularly the peak salinity errors around 14 and 19–21 August. Although some discrepancies still linger in the weak constraints analysis (e.g., days 5 and 8 near the surface), it shows a further reduction in the errors: the peak errors around 14 August have disappeared and those around 19–21 August are significantly reduced in size and magnitude.

4. Fit metric

A global measure of the fit to the observations is given by

$$J_{\mathrm{FIT}} = \frac{1}{M}\sum_{m=1}^{M}\frac{|y_m - H_m X^a|}{\sigma_m}, \qquad (1)$$

where M is the total number of assimilated observations, y_m is the mth observation, X^a is the analysis trajectory, H_m is the observation operator associated with y_m, and σ_m is the observation standard deviation. Because the assimilation is expected to fit the observations to within their prescribed standard deviation, J_{FIT} is expected to be less than 1 for each assimilation cycle. The analysis trajectory in (1) can be replaced by the free-run trajectory in order to assess the latter's accuracy (i.e., how close the free run is to the observations before assimilation). Since the observations are binned in time increments of 6 h, J_{FIT} can be computed over time to examine the evolution of the fit to the observations by the analysis and the free run. Results in Fig. 7 show that the weak constraint analysis generally fits the assimilated temperature and salinity observations to within a standard deviation. The strong constraints also fit the assimilated observations to within a standard deviation, but only initially. As time progresses, the fit becomes less accurate, mostly for temperature. This less accurate fit from the strong constraints could be the result of fewer degrees of freedom (compared to the weak constraints) and the presence of frequent relaxation and an upwelling event in the second half of the assimilation window. The fit to the assimilated salinity observations is similar in both the weak and strong constraint experiments throughout the assimilation window, generally within one standard deviation, except for during the periods 11–13, 17, and 22–23 August.

As for the independent observations, the fit to temperature is within a standard deviation from the beginning of the assimilation window to about 10 August, for both strong and weak constraint experiments. The temperature metric values then start to slowly deviate

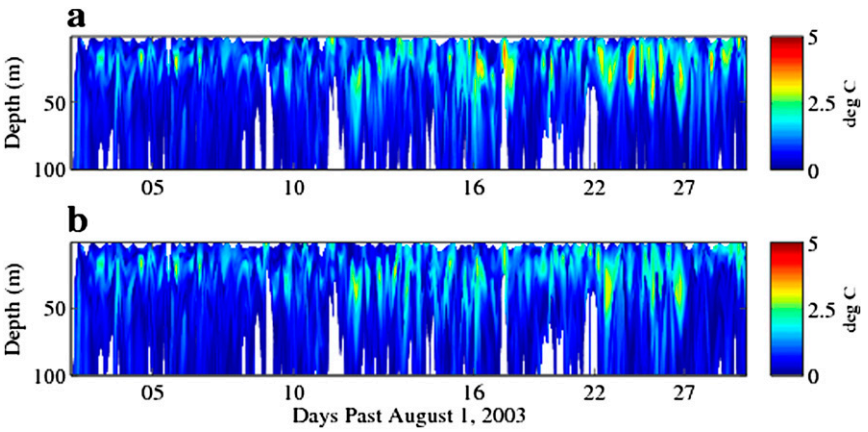

FIG. 8. Absolute temperature discrepancies from nonassimilated observations for (a) the original and (b) the longer correlations weak constraint assimilation experiments.

from the target value of one until 18 August, when they reach 1.3 and 1.6 standard deviations for the weak and strong constraints, respectively. From 18 to 30 August the fit tends to grow, reaching 1.9 (1.7) standard deviations on 29 (25) August for the strong (weak) constraints. The fit metric for nonassimilated salinity observations is similar for both strong and weak constraint solutions, and is almost always greater than the target value of one, occasionally peaking at about 1.6.

The less accurate fit to nonassimilated observations seems to contradict the accurate fit to the assimilated observations and the expectation that the assimilation should also fit independent observations located away from the assimilated ones. One should keep in mind that the assimilated observations were specifically selected in such a way that only one observation was retained within each time–space decorrelation scale. Given the moderate flow in the model domain, it can be argued that the fit to nonassimilated observations is less accurate because the information spreads slowly from the observation locations to other parts of the domain, an outcome that can be reversed either by selecting more observations to be assimilated or longer decorrelation scales. This hypothesis was examined by carrying out a weak constraint experiment with a spatial decorrelation scale of 50 km instead of 30 km, while the observations, initial conditions, and model error standard deviations are unchanged. Temperature analysis errors for nonassimilated observations were compared to the corresponding errors from the original weak constraint experiment. It is shown in Fig. 8 that marginal improvements in the analysis error with the longer scales were obtained. It is arguable that further reduction of these discrepancies could have been achieved with even longer correlation scales or higher initial conditions and model errors. However, both the correlation scales and the error levels cannot be adjusted arbitrarily for the sole purpose of fitting observations. They also have to be rigorously assessed and validated. Such an effort is beyond the scope of this study.

The assimilation system's ability to fit the observations is further examined statistically by comparing the differences between the observations and the free-running model, as well as the strong and the weak constraint analyses for both the assimilated and nonassimilated observations at all times. Elements of these difference vectors are grouped by comparing their magnitudes to the observation standard deviations in the following manner: all elements with an absolute value smaller than a standard deviation are binned together, and so are all elements whose absolute value is between one and two standard deviations, and so on. The number of elements in each bin is then converted into a percentage of the number of assimilated and nonassimilated observations, respectively. The results are plotted as a cumulative bar chart in Fig. 9 and show that the assimilated solution fits 75% and 93% of the observations to within one and two standard deviations, respectively, for the weak constraints. The corresponding numbers are 65% and 86% for the strong constraints, and 45% and 66% for the free run. These numbers are significantly lower for the nonassimilated observations. The weak constraint solutions fit 64% and 84% of the nonassimilated observations within one and two standard deviations, respectively, while the corresponding numbers for the strong constraints are 60.5% and 81%, and 50% and 71% for the free-running model.

5. Conclusions

Strong and weak constraint 4DVAR experiments in Monterey Bay were carried out using the observations collected during AOSN II and the linearized and adjoint

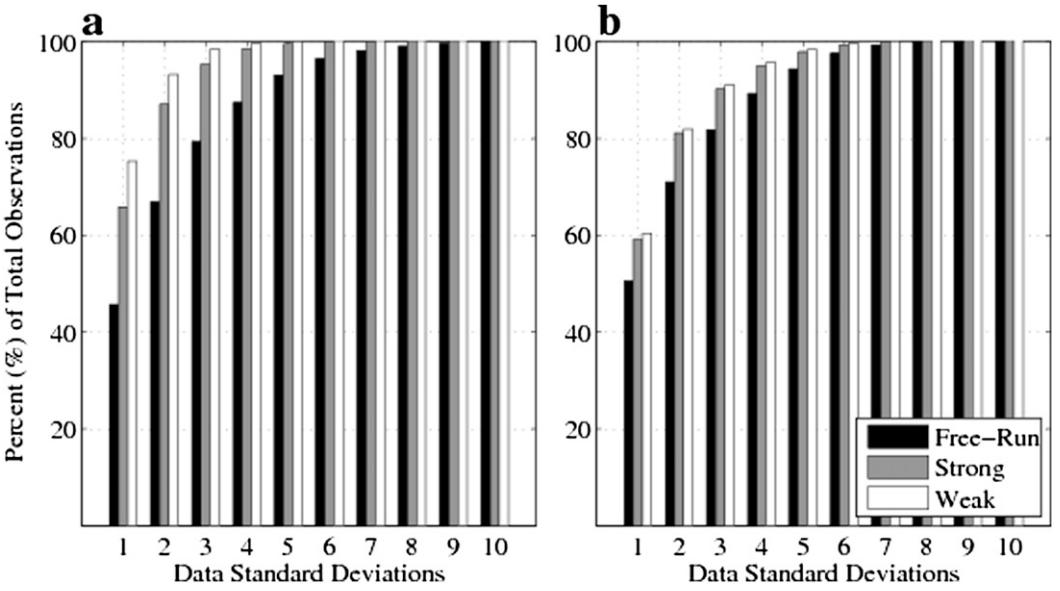

FIG. 9. Cumulative bar chart showing the percentage of the number of observations that are matched by the free-running model (black), and the strong constraints (gray), and weak constraints (white) as a function of the number of observation standard deviations, for the (a) assimilated and (b) nonassimilated observations.

NCOM. Starting from a free-run solution that completely misrepresented both the data and the dynamics of the region during the selected time period, the assimilation was able to accurately fit the assimilated data. As should be expected, the fit to the assimilated observations was more accurate for the weak than the strong constraints. Also, contrary to the free run, the upwelling and relaxation events that dominate the dynamics of the region were accurately described by both strong and weak constraint analyses, which benefited from good observation coverage of the domain and a robust assimilation system. To avoid redundancy, some glider profiles were withheld from the assimilation and used for evaluation. The analysis fit the withheld observations accurately in the first half of the assimilation window, but with less accuracy than the assimilated observations in the second half, which were composed of transitions from upwelling to relaxation and back to upwelling. This was also due in part to the way the assimilated observations were selected and the slow to moderate flow in the model dynamics.

The analysis was also evaluated against independent observations from M1. The location was chosen not only because of the availability of observations, but also because of the strong correlation between the recorded temperatures and the observed wind stress forcing. Both the strong and weak constraint assimilations were able to accurately reproduce the observed temperatures. Also, analysis discrepancies showed that the strong constraint assimilation was able to significantly, but not completely, reduce the salinity errors, particularly the peak errors around 14 August and 19–21 August. The weak constraint analysis was able to further reduce these salinity errors.

Quantitatively and qualitatively, the results from the experiments show that the assimilated solutions fit 75% and 93% of the observations to within one and two standard deviations, respectively, for the weak constraints, with the corresponding numbers being 65% and 86% for the strong constraints, and 45% and 66% for the free run. These numbers are significantly lower for the nonassimilated observations. The weak constraint solutions fit 64% and 84% of the nonassimilated observations within one and two standard deviations, respectively, while the corresponding numbers for the strong constraints are 60.5% and 81%, and 50% and 71% for the free-running model. It can be argued that longer correlation scales and slightly higher model errors, especially in the second half of the assimilation window, could have led to a better fit to the independent observations. A weak constraints experiment with longer correlation scales was carried out here and yielded a better fit to the nonassimilated observations. However, correlation scales and model errors cannot be arbitrarily increased and the investigation of their optimal values is beyond the scope of this study.

Acknowledgments. This work was sponsored by the Office of Naval Research Program Element 0601153N as part of the "Exploring Covariances for Ocean Variational

Data Assimilation'' and ''Variational Data Assimilation for Ocean Prediction'' projects. The authors thank the anonymous reviewers whose comments helped improve the quality of the manuscript.

REFERENCES

Barron, C. N., A. B. Kara, H. E. Hurlburt, C. Rowley, and L. F. Smedstad, 2004: Sea surface height predictions from the Global Navy Coastal Ocean Model (NCOM) during 1998–2001. *J. Atmos. Oceanic Technol.,* **21,** 1876–1894, doi:10.1175/JTECH-1680.1.

——, ——, P. J. Martin, R. C. Rhodes, and L. F. Smedstad, 2006: Formulation, implementation and examination of vertical coordinate choices in the Global Navy Coastal Ocean Model (NCOM). *Ocean Modell.,* **11,** 347–375, doi:10.1016/j.ocemod.2005.01.004.

Bennett, A. F., 1992: *Inverse Methods in Physical Oceanography.* Cambridge University Press, 347 pp.

——, 2002: *Inverse Modeling of the Ocean and Atmosphere.* Cambridge University Press, 234 pp.

Chao, Y., and Coauthors, 2009: Development, implementation and evaluation of a data-assimilative ocean forecasting system off the central California coast. *Deep-Sea Res. II,* **56,** 100–126, doi:10.1016/j.dsr2.2008.08.011.

Cummings, J., 2005: Operational multivariate ocean data assimilation. *Quart. J. Roy. Meteor. Soc.,* **131,** 3583–3604, doi:10.1256/qj.05.105.

Haley, P. J., P. F. J. Lermusiaux, W. G. Leslie, and A. R. Robinson, 1999: Harvard Ocean Prediction System (HOPS). [Available online at http://mseas.mit.edu/archive/HOPS/HOPS.html.]

——, and Coauthors, 2009: Forecasting and reanalysis in the Monterey Bay/California Current region for the Autonomous Ocean Sampling Network-II experiment. *Deep-Sea Res. II,* **56,** 127–148, doi:10.1016/j.dsr2.2008.08.010.

Kindle, J. C., R. M. Hodur, S. deRada, J. D. Paduan, L. K. Rosenfeld, and L. Q. Chavez, 2002: A COAMPS™ reanalysis for the Eastern Pacific: Properties of the diurnal sea breeze along the central California coast. *Geophys. Res. Lett.,* **29,** 2203, doi:10.1029/2002GL015566.

Lermusiaux, P. F. J., A. R. Robinson, P. J. Haley, and W. G. Leslie, 2002: Advanced interdisciplinary data assimilation: Filtering and smoothing via error subspace statistical estimation. *Proc. OCEANS 2002,* Vol. 2, IEEE, Biloxi, MS, 795–802, doi:10.1109/OCEANS.2002.1192071.

Liang, X. S., and A. R. Robinson, 2009: Multiscale processes and nonlinear dynamics of the circulation and upwelling events off Monterey Bay. *J. Phys. Oceanogr.,* **39,** 290–313, doi:10.1175/2008JPO3950.1.

Martin, P., 2000: Description of the Navy Coastal Ocean Model Version 1.0. NRL Rep. NRL/FR/7322-00-9961, 42 pp.

Ngodock, H., and M. Carrier, 2014: A 4DVAR system for the Navy Coastal Ocean Model. Part I: System description and assimilation of synthetic observations in Monterey Bay. *Mon. Wea. Rev.,* **142,** 2085–2107, doi:10.1175/MWR-D-13-00221.1.

Ramp, S. R., and Coauthors, 2009: Preparing to predict: The Second Autonomous Ocean Sampling Network (AOSN-II) experiment in the Monterey Bay. *Deep-Sea Res. II,* **56,** 68–86, doi:10.1016/j.dsr2.2008.08.013.

Robinson, A. R., 1999: Forecasting and simulating coastal ocean processes and variabilities with the Harvard Ocean Prediction System. *Coastal Ocean Prediction,* C. N. K. Mooers, Ed., Coastal and Estuarine Studies Series, Amer. Geophys. Union, 77–100.

——, H. G. Arango, A. Warn-Varnas, W. G. Leslie, A. J. Miller, P. J. Haley Jr., and C. J. Lozano, 1996: Real-time regional forecasting. *Modern Approaches to Data Assimilation in Ocean Modelling,* P. Malanotte-Rizzoli, Ed., Elsevier Oceanography Series, Elsevier Science, 377–412.

Shchepetkin, A. F., and J. C. McWilliams, 2005: The Regional Oceanic Modeling System: A split-explicit, free-surface, topography-following-coordinate ocean model. *Ocean Modell.,* **9,** 347–404, doi:10.1016/j.ocemod.2004.08.002.

Shulman, I., C. R. Wu, J. K. Lewis, J. D. Paduan, L. K. Rosenfeld, J. C. Kindle, S. R. Ramp, and C. A. Collins, 2002: High resolution modeling and data assimilation in The Monterey Bay. *Cont. Shelf Res.,* **22,** 1129–1151, doi:10.1016/S0278-4343(01)00100-5.

——, and Coauthors, 2009: Impact of glider data assimilation on the Monterey Bay model. *Deep-Sea Res. II,* **56,** 188–198, doi:10.1016/j.dsr2.2008.08.003.

——, S. Anderson, C. Rowley, S. DeRada, J. Doyle, and S. Ramp, 2010: Comparison of upwelling and relaxation events in the Monterey Bay area. *J. Geophys. Res.,* **115,** C06016, doi:10.1029/2009JC005483.